A NON-VOLATILE THRESHOLD SENSING SYSTEM USING A FERROELECTRIC Hf_{0.5}Zr_{0.5}O₂ DEVICE AND A LinbO₃ MICROACOUSTIC RESONATOR

Onurcan Kaya, Luca Colombo, Benyamin Davaji, and Cristian Cassella Northeastern University, Electrical Engineering, Boston, MA, USA

ABSTRACT

This work reports a novel threshold sensor system that is able to detect and memorize the occurrence of temperature violations by relying on a 20 nm-thick ferroelectric Hafnium Zirconium Oxide (HZO) varactor and a LiNbO3 shear-horizontal (SH0) Lamb wave microacoustic resonator, both microfabricated in-house. The reported sensor system is driven by a continuous-wave signal at a frequency (fin) slightly detuned from the LiNbO₃ device's resonance frequency (fres~33.3 MHz). When the ambient temperature changes, the voltage at f_{in} across the varactor increases proportionally to the resonator's figureof-merit (FoM), ultimately causing a partial ferroelectric polarization switching of the HZO varactor for a temperature exceeding a certain programmable threshold (T_{th}) . Following such a switching event, the capacitance (C_T) of the HZO varactor experiences a sudden change, causing a non-volatile 0.75-1 MHz shift of the read-out resonance frequency ($f_{read} \sim 260 \text{ MHz}$) that is equal to the resonance frequency of an LC-tank formed by a lumped inductor and by the series of C_T with the LiNbO₃ device's capacitance (C_0) . The ability to generate temperatureinduced non-volatile changes of fread through HZO ferroelectric varactors and microacoustic resonators is demonstrated for the first time in this work, and represents the key to implement a threshold sensing functionality and to memorize the occurrence of any temperature violations.

KEYWORDS

Ferroelectricity, Temperature Threshold Sensing, Hafnium Zirconium Oxide, Lithium Niobate, Acoustic Resonators

INTRODUCTION

Improper refrigeration of food and drugs along the cold chain represents a significant problem, generating threats to human health safety and severe economic losses. Fueled by the Radio-Frequency-Identification (RFID) revolution, several temperature sensing technologies have been developed, aiming at timely identifying and permanently marking any items undergoing temperature violations [1-10]. In this regard, thanks to their superior electromechanical performance and high Temperature-Coefficient-of-Frequency (TCF), various microacoustic temperature sensors have been reported [11, 12]. Such devices can sense their ambient temperature with high sensitivity, yet they cannot be used for threshold sensing. Also, they cannot keep track of any previously occurred temperature violations.

Hafnium Zirconium Oxide (Hf_{0.5}Zr_{0.5}O₂ or HZO) varactors have been used in resistive and capacitive memory applications [13, 14]. This paper leverages an HZO varactor as a readout element in a novel threshold

sensing system. The proposed system relies on a ferroelectric 20 nm-thick HZO varactor and a Lithium Niobate (LiNbO₃) microacoustic RF resonator. The LiNbO₃ resonator is used as a temperature-sensing element and the HZO varactor is utilized in a series LC resonant circuit as a non-volatile memory element to detect and memorize the occurrence of temperature violations. In the proposed system the LiNbO3 microacoustic resonator is driven by a continuous-wave signal at a frequency ($f_{in} = 33$ MHz) that is very close to the device's resonance frequency (fres~ 33.3 MHz), and the LC readout circuitry resonates at around 260 MHz (fread). Ambient temperature change shifts the resonance frequency of the microacoustic resonator causing a passive voltage amplification across the ferroelectric varactor. When the ambient temperature change is larger than the designed threshold value, the voltage across the HZO varactor becomes large enough to initiate the ferroelectric switching, which creates a nonvolatile 0.75-1 MHz shift of fread.

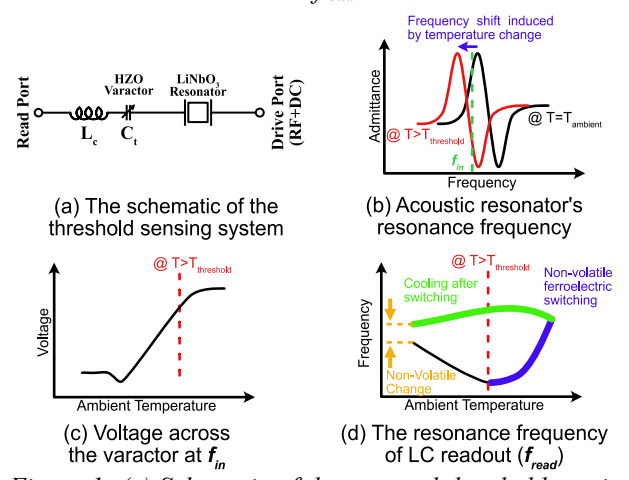


Figure 1: (a) Schematic of the reported threshold sensing system; (b, c, and d) Summary of the working principle of our reported threshold sensing system; (b) The acoustic resonator is excited by a continuous-wave signal with a frequency (fin) close to its resonance frequency. When the ambient temperature changes, the resonance frequency of the resonator shifts left, (c) Such a shift in the resonance frequency of the acoustic resonator triggers a passive voltage amplification across the varactor at fin. (d) When the voltage across the HZO varactor increases the resonance frequency (fread) of the LC-readout circuitry decreases until the voltage becomes large enough to initiate the ferroelectric switching of the HZO varactor (black line segment). When the ambient temperature exceeds a certain threshold temperature ($T_{threshold}$) the voltage across the varactor becomes large enough to trigger the ferroelectric switching (blue line segment). As a result, fread undergoes a non-volatile change, allowing to capture and memorize the occurrence of the temperature violation.

DEVICE OPERATION

This system consists of a LiNbO3 microacoustic resonator, a Hf_{0.5}Zr_{0.5}O₂ (HZO) ferroelectric varactor and an inductor (Fig. 1-a). Figs. 1-b,c,d summarize the basic operating principle of the system. The LiNbO₃ microacoustic resonator is used as a temperature sensing element and it is excited with a continuous-wave signal at a frequency (f_{in}) , which is slightly detuned from the resonance frequency of the resonator (f_{res}). Meanwhile, the inductor forms a series LC resonant circuit with the HZO varactor and the static capacitance of the LiNbO3 device, whose resonance frequency (fread) is used as a readout parameter. When the ambient temperature changes, the LiNbO₃ resonator's resonance frequency shifts to the left (Fig. 1-b). This triggers a passive amplification of the varactor's voltage at fin (Fig. 1-c) that induces a ferroelectric switching when the temperature exceeds a certain threshold (T_{th}) that can be programmed by setting f_{in} . As a result, f_{read} undergoes a non-volatile change, allowing one to capture and memorize the occurrence of any temperature violations (Fig. 1-d).

FABRICATION

The fabrication flow of the LiNbO₃ resonator is given in Fig. 2 (a). The process started with a 2.5 um thin film X-cut LiNbO₃ on a high resistivity silicon wafer. The thin film LiNbO₃ was bonded to the silicon wafer via Surface Activated Bonding (SAB) and thinned to the desired thickness (performed by NGK, Inc.). Then the release pits were formed by using ion milling, followed by the sputter deposition and patterning by lift-off of a 400 nm-thick AlSiCu layer to form the resonator's top electrodes.

Finally, the device was released through the XeF₂ isotropic etch.

The fabrication flow of the HZO varactor is given in Fig. 2 (b). A low-resistivity silicon wafer with a 150 nm thermal oxide was used as the varactor's substrate. 100 nmthick Platinum (Pt) bottom electrodes were sputtered and patterned via lift-off. At this step, to minimize any fencings along the bottom electrode's edges, a bi-layer lift-off process was optimized. It is worth mentioning that the HZO device's bottom electrode was designed to be slightly wider than its top electrode to decrease the number of overlapping edges. Then, a 20 nm thick ferroelectric HZO layer and a 3 nm thick Al₂O₃ capping layer were deposited using Atomic Layer Deposition. The binary HZO layer was deposited by alternating the pulses of (dimethylamido) hafnium (TFMAHf) and (dimethylamino) zirconium (TDMAZr) precursors, each of which is followed by water pulses as the O₂ source. The Al₂O₃ layer was instead deposited using alternating pulses of trimethylaluminium (TMA) and water precursors. Next, vias to reach the bottom electrode were formed through a dry etch process. Finally, 150 nm thick gold top electrodes were deposited using e-beam evaporation. After the fabrication, HZO varactors were annealed using a rapid thermal processor (RTP) under vacuum in a Nitrogen (N₂) environment for 40 seconds at 400°C.

SEM images of the fabricated LiNbO₃ microacoustic resonator and HZO varactor are shown in Fig. 2 (c) and (d), respectively. As can be seen from Fig. 2 (c) the resonator consists of 7 identical parallel resonators with a pitch of 57 µm. Structural layers of the HZO varactor are highlighted in Fig. 2 (d), together with close-up views of the overlap area and of the via the region.

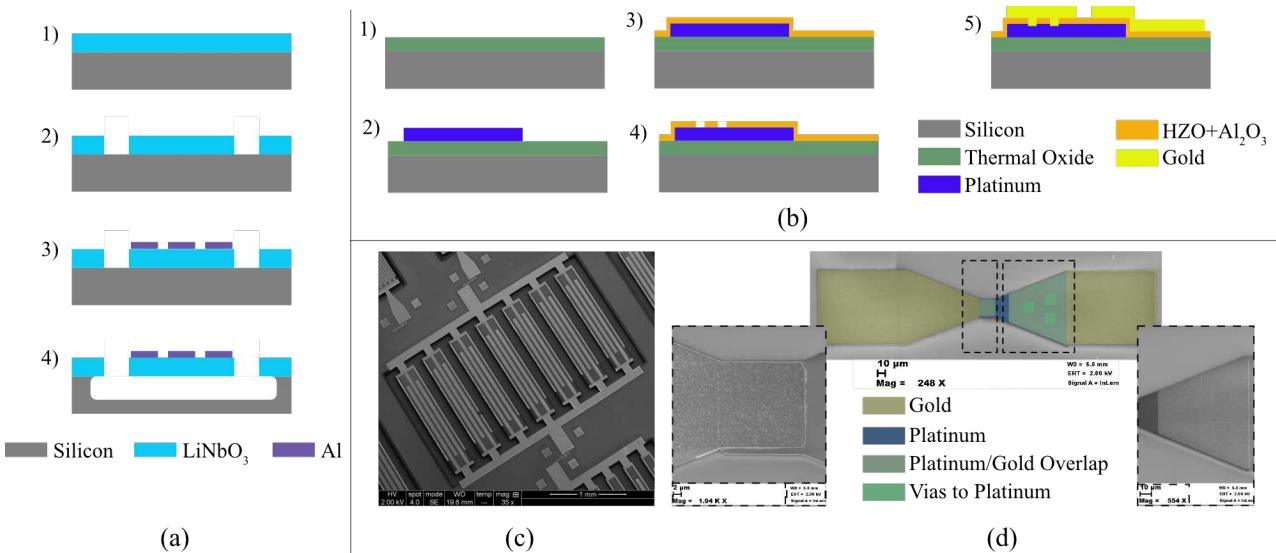


Figure 2: (a) Fabrication flow of the LiNbO3 resonator; (1) The fabrication of the LiNbO3 resonator relies on a 2.5 µm thin film X-cut LiNbO3 wafer, bonded to the silicon substrate via Surface Activated Bonding and thinned to the desired thickness. (2) We started by forming the release pits through ion milling. (3) Then a 400 nm Al top electrode was sputtered and patterned through lift off. (4) Finally, the device was released through XeF2 isotropic etch; (b) Fabrication flow of the HZO varactor; (1) A silicon wafer with a 150 nm thermal oxide was used as substrate. (2) A 100 nm thick Platinum bottom electrode was sputtered and patterned by lift-off. (3) Then, 20 nm HZO and 3 nm Al₂O₃ films were deposited using Atomic Layer Deposition. (4) Following this step, the vias were formed through the HZO film to reach the bottom Pt electrode. (5) Finally, a 150 nm top gold electrode was deposited by using e-beam evaporation. After the fabrication, the HZO varactor was annealed through a Rapid Thermal Processor in an N₂ environment for 40 seconds at 400°C; (c) SEM image of the fabricated LiNbO₃ resonator; (d) SEM image of the fabricated HZO varactor.

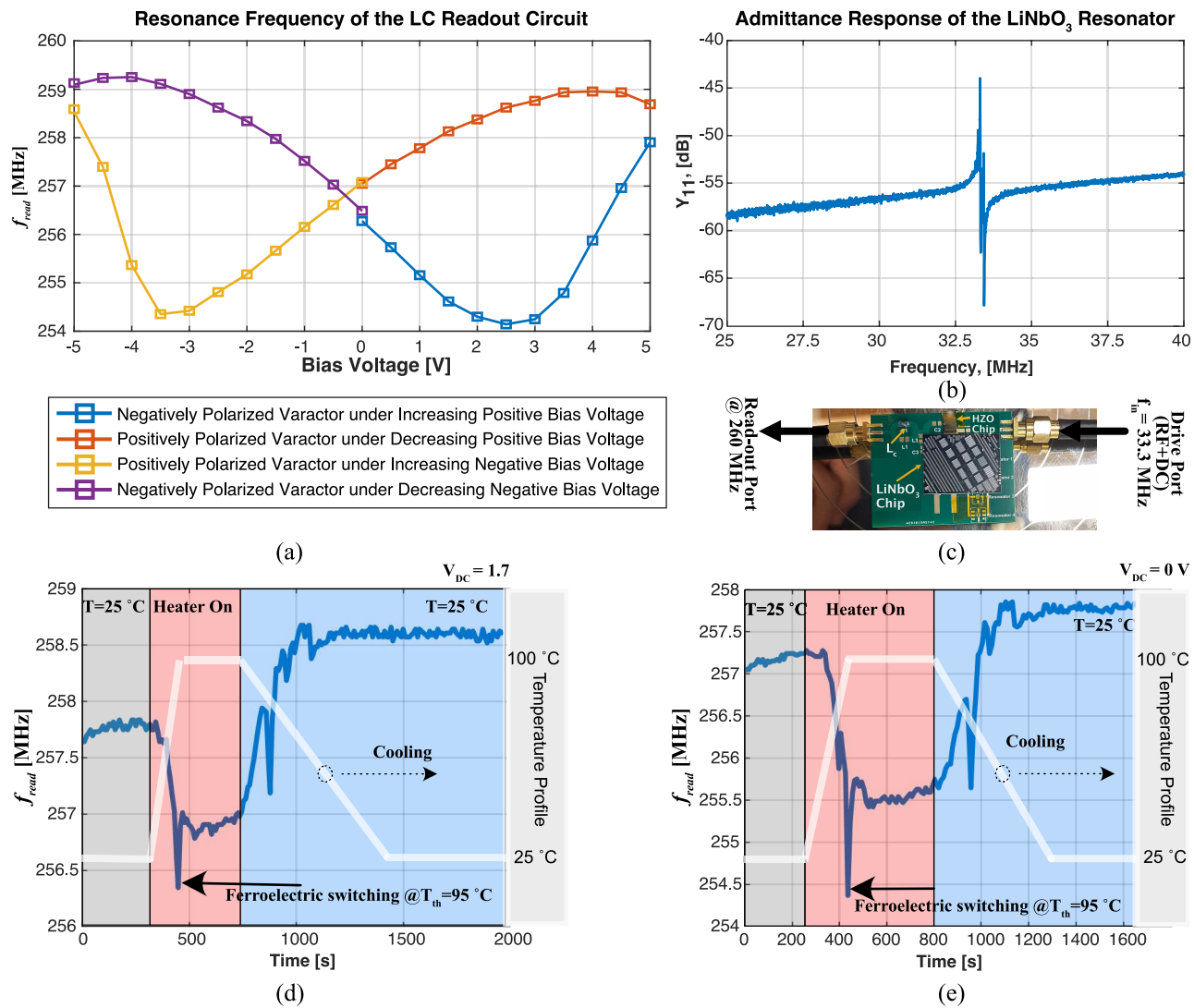


Figure 3: (a) Measured trend of f_{read} vs. the applied DC voltage, extracted at ambient temperature. The varactor was initially negatively polarized, and it was subjected to a positive bias voltage (shown by the blue line segment). The resonance frequency decreased until ferroelectric switching occurs, followed by a rapid and sharp increase. Next, the bias voltage was brought back to zero (shown by the orange line segment). At that point, the varactor was positively polarized. The procedure was repeated for negative bias signals (yellow and purple curves). (b) Admittance response of the LiNbO3 resonator. (c) Top-view picture of the assembled threshold sensing system on top of a PCB. In order to characterize its threshold sensing performance, the system was DC-biased and was excited at f_{in} from one of its ports (the "Drive port") while tracking f_{read} from the other port (the "Read port") by using a vector network analyzer; (d,e) Temperature response of the reported threshold sensing system under two DC-biasing voltages (1.7 V (d) and 0 V (e)). The right curve was obtained after applying a reset voltage pulse to reset the ferroelectric varactor's state. The temperature was increased up to $100\,^{\circ}$ C and later brought back to $25\,^{\circ}$ C. Evidently, a ferroelectric switching occurred producing a sudden notch when the temperature exceeded $95\,^{\circ}$ C. Moreover, as the temperature re-reached $25\,^{\circ}$ C, the f_{read} value became different from the original value. Such a non-volatile shift is the key to recognize that a violation has occurred.

EXPERIMENTAL RESULTS

The two key components of the threshold sensing system, *i.e.* the LC readout circuit and the LiNbO₃ microacoustic resonator, were first tested separately at ambient temperature. Fig.1-a shows the ferroelectric behavior of the f_{res} under a swept DC bias voltage at room temperature. Initially, the ferroelectric varactor was negatively polarized, and it was subjected to a positive bias voltage. The resonance firstly decreased until the varactor's ferroelectric domains start switching. The ferroelectric switching started at around 2.5 V, above

which the resonance frequency started to increase sharply (see the blue line in Fig. 1-a). At that point, most of the ferroelectric domains in the HZO varactor were positively polarized. After that, the DC bias was brought back to 0 V. The resonance frequency of the LC circuit decreased following the orange curve. Then the same procedure was repeated for the negative DC bias values. The behavior of the LC circuit's resonance frequency for negative DC bias voltages is shown by the yellow and purple curves. Fig. 2-b shows the admittance response of the LiNbO₃ resonator. As can be seen, its resonance frequency was measured around 33.3 MHz.

The threshold system was assembled on a Printed Circuit Board (PCB), as shown in Fig. 3-c. The system was DC-biased and excited from the drive port at a frequency fin slightly detuned from the resonance frequency of the resonator, while tracking f_{read} from the read-port by using a network analyzer. The temperature responses of the reported threshold sensing system were obtained under two different DC-biasing voltages of 1.7 V and 0 V, and are shown in Fig. 3- d and Fig. 3-e. The system was heated up to 100 °C and then cooled down to room temperature again. During our experiment we found the passive voltage amplification across the varactor to become large enough when the temperature exceeded 95°C, after which a ferroelectric partial switching occurred, producing a sudden notch on fread. Even more, when the temperature rereached 25°C, we found f_{read} to be different from its original value. Such a non-volatile change is the key to recognizing that a temperature violation has occurred.

CONCLUSIONS

In this work, a novel temperature threshold sensing system based on a LiNbO₃ microacoustic resonator and a ferroelectric HZO varactor was reported. The system uses the LiNbO₃ resonator as a temperature sensing element and leverages the HZO varactor as a non-volatile element of an LC tank whose resonance frequency was used as a read-out parameter. The proposed system was implemented on top of a PCB and its temperature response was measured under two different DC-biasing voltages. The obtained results revealed that the combination of a ferroelectric element with a MEMS device enables the realization of sense, computation, and storage functions.

ACKNOWLEDGEMENTS

This work has been funded by the National Science Foundation CCF-FET program (Grant #2103351 & #2103091). The authors wish to thank the staff of the George J. Kostas Nanoscale Technology and Manufacturing Research Center at Northeastern University for assistance in the device fabrication.

REFERENCES

- [1] G. Bruckner, J. Bardong, C. Gruber, and V. Plessky, "A Wireless, Passive ID Tag and Temperature Sensor for a Wide Range of Operation," *Procedia Engineering*, vol. 47, pp. 132-135, 2012/01/01/2012, doi: https://doi.org/10.1016/j.proeng.2012.09.102.
- [2] H. Campanella, M. Narducci, S. Merugu, and N. Singh, "Dual MEMS Resonator Structure for Temperature Sensor Applications," *IEEE Transactions on Electron Devices*, vol. 64, no. 8, pp. 3368-3376, 2017, doi: 10.1109/TED.2017.2708129.
- [3] R. Bhattacharyya, C. Floerkemeier, and S. Sarma, "RFID tag antenna based temperature sensing," in 2010 IEEE International Conference on RFID (IEEE RFID 2010), 14-16 April 2010 2010, pp. 8-15, doi: 10.1109/RFID.2010.5467239.
- [4] I. Zalbide, E. D. Entremont, A. Jiménez, H. Solar, A. Beriain, and R. Berenguer, "Battery-free wireless sensors for industrial applications based on UHF RFID technology," in SENSORS, 2014 IEEE, 2-5 Nov. 2014

- 2014, pp. 1499-1502, doi: 10.1109/ICSENS.2014.6985299.
- [5] T. T. Thai *et al.*, "Design and Development of a Novel Passive Wireless Ultrasensitive RF Temperature Transducer for Remote Sensing," *IEEE Sensors Journal*, vol. 12, no. 9, pp. 2756-2766, 2012, doi: 10.1109/JSEN.2012.2201463.
- [6] C. Ghouila-Houri et al., "MEMS high temperature gradient sensor for skin-friction measurements in highly turbulent flows," in 2019 IEEE SENSORS, 27-30 Oct. 2019 2019, pp. 1-4, doi: 10.1109/SENSORS43011.2019.8956802.
- [7] A. Jiménez-Sáez *et al*, "Chipless Wireless High Temperature Sensing Based on a Multilayer Dielectric Resonator," in *2019 IEEE SENSORS*, 27-30 Oct. 2019 2019, pp. 1-4, doi: 10.1109/SENSORS43011.2019.8956863.
- [8] H. M. E. Hussein and C. Cassella, "Giant Sensitivity through Fully-Passive and Chip-Less Parametric Temperature Sensors," in 2020 IEEE SENSORS, 25-28 Oct. 2020 2020, pp. 1-4, doi: 10.1109/SENSORS47125.2020.9278907.
- [9] H. M. E. Hussein, M. Rinaldi, M. Onabajo, and C. Cassella, "Capturing and recording cold chain temperature violations through parametric alarmsensor tags," *Applied Physics Letters*, vol. 119, no. 1, p. 014101, 2021/07/05 2021, doi: 10.1063/5.0054022.
- [10] H. M. E. Hussein, M. Rinaldi, M. Onabajo, and C. Cassella, "A chip-less and battery-less subharmonic tag for wireless sensing with parametrically enhanced sensitivity and dynamic range," *Scientific Reports*, vol. 11, no. 1, p. 3782, 2021/02/12 2021, doi: 10.1038/s41598-021-82894-x.
- [11] X.-G. Tian *et al*, "High-resolution, high-linearity temperature sensor using surface acoustic wave device based on LiNbO₃/SiO₂/Si substrate," *AIP Advances*, vol. 6, no. 9, p. 095317, 2016/09/01 2016, doi: 10.1063/1.4963797.
- [12] J. Zhao *et al.*, "The research of dual-mode film bulk acoustic resonator for enhancing temperature sensitivity," *Semiconductor Science and Technology*, vol. 36, no. 2, p. 025018, 2021/01/06 2021, doi: 10.1088/1361-6641/abd15c.
- [13] S. Jadhav et al, "HZO-based FerroNEMS MAC for inmemory computing," Applied Physics Letters, vol. 121, no. 19, p. 193503, 2022/11/07 2022, doi: 10.1063/5.0120629.
- [14] V. Gund *et al.*, "Multi-level Analog Programmable Graphene Resistive Memory with Fractional Channel Ferroelectric Switching in Hafnium Zirconium Oxide," in 2022 Joint Conference of the European Frequency and Time Forum and IEEE International Frequency Control Symposium (EFTF/IFCS), 24-28 April 2022 2022, pp. 1-4, doi: 10.1109/EFTF/IFCS54560.2022.9850768.

CONTACT

*Onurcan Kaya, tel: +1-605-2520066; kaya.on@northeastern.edu *Cristian Cassella, tel: +1-267-9925507; c.cassella@northeastern.edu